Jurnal Kejuruteraan 38(4) 2026: 2043-2058
https://doi.org/10.17576/jkukm-2026-38(4)-38

Green Synthesis of ZnO and Fe_2O_3 Nanoparticles for the Removal of Crystal Violet and Bromophenol Blue Dyes

Hitesh Pareek[a], Pankaj Kumar Jain[a*], Prama Esther Soloman[a], Madhu Yadav[b] & Chhagan Lal[b,c]

[a]*Department of Environmental Science, Indira Gandhi Centre for Human Ecology,*

Environmental and Population Studies, University of Rajasthan, Jaipur, India

[b]*Department of Physics, University of Rajasthan, Jaipur, India*

[c]*Centre for Non-Conventional Energy Resources, University of Rajasthan Jaipur, India*

[*]*Corresponding author: pankajbio2001@gmail.com*

Received 24 April 2025, Received in revised form 25 March 2026
Accepted 25 April 2026), Available online 30 July 2026

ABSTRACT

Green synthesis of metal oxide nanoparticles using plant extracts has emerged as an environmentally friendly and sustainable alternative to conventional chemical methods. In the present study, ZnO and Fe_2O_3 nanoparticles were synthesized via a plant-mediated route and systematically characterized using UV–Visible spectroscopy, Fourier Transform Infrared Spectroscopy (FTIR), High-Resolution Transmission Electron Microscopy (HRTEM), X-ray Diffraction (XRD), and X-ray Photoelectron Spectroscopy (XPS) to confirm their structural, morphological, and chemical properties. The removal efficiency of the synthesized nanoparticles was evaluated against two model dyes, crystal violet and bromophenol blue, with initial concentrations of 5mg/L and 10mg/L, respectively, under ambient conditions over a 24-hour reaction period. The results demonstrated distinct performance trends for the two nanomaterials. Fe_2O_3 nanoparticles exhibited higher removal efficiency toward crystal violet, achieving a maximum removal efficiency of 84.32%. In contrast, ZnO nanoparticles showed enhanced removal capability for bromophenol blue, reaching up to 98.15% removal under identical experimental conditions. These findings indicate that removal efficiency is influenced by both the physicochemical properties of the nanoparticles and the nature of the dye molecules. The comparative evaluation highlights the selective applicability of ZnO and Fe_2O_3 nanoparticles for targeted dye removal in wastewater treatment applications.

Keywords: Zinc oxide nanoparticles; iron oxide nanoparticles; green synthesis; characterization; dye removal

INTRODUCTION

Providing safe drinking water to everyone is currently the biggest problem facing humanity because it is a basic human need and an essential part of existence. According to the World Health Organization, approximately 2.2 billion people globally lack access to safely managed drinking water services (Gordon et al. 2023). However, the need for new technological innovations to fulfill water demands has been spurred by growing demand and falling water tables in almost every location. The textile and dye industry, which consumes a large amount of water to prepare dyes, is perhaps one of the most polluting industries in the world (Kaur et al. 2018; Kovács et al. 2018). The textile sector is estimated to account for nearly 20% of global industrial wastewater discharge, with dye concentrations in effluents commonly ranging from 10 to 200 mg/L (Kant & Kant 2012). Many dye-containing effluents released by industry have been reported to contain carcinogens, algal bloom promoting agents, oxygen demanding water pollutants, and a variety of water-borne diseases. Numerous colored effluents produced by these companies are a significant source of pollution and are challenging for conventional technology to break down (Razavi et al. 2021). The complex aromatic molecular structures and synthetic origin of these dyes render them highly stable and resistant to biodegradation (Tripathi et al. 2023).

Many physical and chemical remediation strategies, such as flocculation, electro-coagulation, ultraviolet

degradation, and adsorption techniques such as activated carbon have been used extensively to get rid of dye pollution over the last ten years. Nevertheless, the drawbacks of these methods prohibit their widespread application (Kumar et al. 2011; Mahmoodi et al. 2011; Singh & Dhaliwal, 2020). Coagulation and flocculation generate secondary sludge requiring disposal, adsorption processes demand regeneration of sorbents, and advanced oxidation techniques often involve high energy consumption and operational costs (Tripathi et al. 2023).

Thanks to developments in nanotechnology, metal nanoparticles have been successfully demonstrated for the treatment of wastewater. Nanomaterials are quickly discovering new applications due to their unique physicochemical properties, including high surface area, smaller size, and tunable morphology. Because of the above-mentioned inherent characteristics, nanomaterials are ideal for catalytic degradation (Nagar & Devra, 2019; Veréb et al. 2020). Metal oxide nanoparticles promote dye degradation primarily through surface-mediated redox reactions and the generation of reactive oxygen species capable of mineralizing complex organic molecules. (Aina et al. 2025) Biogenically generated nanoparticles can be extremely important when environmentally friendly methods are chosen to remove the colors from wastewater (Bibi et al. 2017; Singh et al. 2017).

Metal oxide nanoparticles have become effective tools for degrading pollutants in environmental remediation, one of the many fields that nanotechnology has transformed. Because of their catalytic qualities, zinc oxide (ZnO) and iron oxide (Fe_2O_3) nanoparticles have attracted interest for their potential in the treatment of organic dyes. ZnO nanoparticles are widely investigated due to their strong oxidizing potential, chemical stability, and suitability for advanced oxidation processes, whereas Fe_2O_3 nanoparticles offer visible-light activity and magnetic recoverability, enabling easier post-treatment separation. (Soni et al. 2025) Ethnomedicinal plants, which have long been utilized for their therapeutic qualities in a variety of cultures, provide a sustainable route for nanoparticle synthesis. Although numerous studies report individual metal oxide systems for dye removal, comparative evaluations of biogenically synthesized ZnO and Fe_2O_3 nanoparticles under identical experimental conditions remain relatively limited. (Tripathi et al. 2023) With a focus on crystal violet and bromophenol blue, this work investigates the creation of ZnO and Fe_2O_3 nanoparticles using plant extracts and assesses how well they degrade dyes. This study intends to advance wastewater treatment while offering an eco-friendly substitute for traditional nanoparticle manufacturing by utilizing green synthesis techniques.

MATERIALS AND METHODS

PREPARATION OF PLANT EXTRACTS

Twenty grams of dried leaf powder were mixed in one hundred milliliters of distilled water to create the plant extracts. Aqueous extraction is commonly employed in green synthesis protocols to obtain bioactive phytochemicals that act as reducing and stabilizing agents (Iravani, 2011). The mixture was filtered and used for the synthesis of nanoparticles after being stirred for two hours at 40°C using a magnetic stirrer. Mild thermal treatment during extraction enhances the release of phenolic and flavonoid compounds responsible for nanoparticle reduction (Ritu et al. 2023).

PREPARATION OF ZINC OXIDE NANOPARTICLES

Zinc oxide nanoparticle synthesis was carried out using leaf extract of *Aegle marmelos*. Zinc acetate solution was used as the precursor salt to prepare Zinc Oxide nanoparticles. Zinc acetate is widely used as a precursor in green synthesis of ZnO nanoparticles due to its high solubility and controlled hydrolysis behaviour (Aina et al. 2025). In the zinc acetate solution, leaf extract was mixed drop by drop while constantly stirring on a magnetic stirrer. Dropwise addition under continuous stirring facilitates uniform nucleation and controlled growth of ZnO nanoparticles (Akintelu & Folorunso 2020). The appearance of brownish-yellow colour indicated the synthesis of ZnO nanoparticles. Visual color change during synthesis is commonly attributed to nanoparticle formation and changes in surface plasmon resonance behaviour (Ritu et al. 2023). The resulting solution was centrifuged at 10,000 rpm for 15 minutes. The pellet was washed 3 times with distilled water and 1 time with ethanol by centrifuging at 5000 rpm for 5 minutes in each cycle. The resulting pellets were kept in a muffle furnace at 500°C for 30 minutes for calcination. Calcination at elevated temperatures enhances crystallinity and removes residual organic phytochemicals from the nanoparticle surface (Kolodziejczak-Radzimska & Jesionowski, 2014). The obtained nanoparticles were stored for further use (Sharmila and Gayathri 2014).

PREPARATION OF IRON OXIDE NANOPARTICLES

The iron oxide nanoparticles (Fe_2O_3) synthesis, using extract of leaves of *Mangifera indica* was carried out. Ferric chloride is commonly employed as a precursor salt in green synthesis of iron oxide nanoparticles due to its high reactivity and ease of hydrolysis (Saif et al. 2016). Briefly, after preparing an aqueous solution of ferric chloride, 20 ml of the previously prepared plant extract was added drop

wise to the solution. Controlled dropwise addition promotes uniform nucleation and prevents rapid agglomeration during nanoparticle formation (Ebrahiminezhad et al. 2018). A 0.10 M NaOH was used to maintain the pH of the reaction solution at 11 (Mahdavi et al. 2013). The whole reaction process was carried out with constant stirring at 300 rpm at room temperature (~25 °C) (Iravani, 2011). The iron oxide nanoparticle solution was then centrifuged for 20 min at 13,000 rpm. The separated nanoparticles were then cleaned with DI water three times followed by ethyl alcohol to remove any unreacted biomolecules before drying for 24 h at 40 °C (Yadwade et al. 2021). The clean and dried Fe_2O_3 nanoparticles were stored for subsequent use.

CHARACTERIZATION OF THE SYNTHESIZED NANOPARTICLES

Synthesized nanoparticles were characterized using UV-Visible Spectroscopy, Fourier Transform Infrared Spectroscopy, High-Resolution Transmission Electron Microscopy, X-ray Photoelectron Spectroscopy, and X-ray Diffraction techniques at the Material Research Centre, MNIT, Jaipur, Rajasthan. A UV-vis spectrophotometer with a wavelength range of 200-900 nm was used to evaluate the optical absorption characteristics and band gap behavior of nanoparticles (Kolodziejczak-Radzimska & Jesionowski, 2014), followed by the FTIR analysis on a FT-IR Spectrum range of 4000 to 400 cm^{-1} using a Perkin Elmer FT-IR Spectrum 2, to identify functional groups and confirm the presence of phytochemicals associated with nanoparticle surface stabilization (Iravani, 2011). HRTEM analysis was performed to determine the size, dimensions, and other morphological characteristics of the nanoparticles (Ramesh et al. 2015). XPS was performed to determine the oxidation state and elemental composition of the material, using the XPS, ESCA+ Omicron Nano Technology (Biesinger, 2017). The crystalline nature and size of the prepared material were analyzed by XRD (Panalytical X Pert Pro X-Ray Diffractometer) (Patterson, 1939).

DETERMINATION OF DYE DEGRADATION POTENTIAL OF THE SYNTHESIZED NANOPARTICLES

The dye degradation experiments were carried out using bromophenol blue (BPB) and crystal violet (CV) as model dyes. A 1% (w/v) stock solution of each dye was prepared and subsequently diluted to obtain working concentrations of 5 mg/L for CV and 10 mg/L for BPB.

For each experiment, 100 mL of the respective dye solution was transferred into test tubes, and ZnO or Fe_2O_3 nanoparticles were added at different dosages of 200, 400, 600, 800, and 1000 µg/mL. The reaction mixtures were vortexed to ensure uniform dispersion of the nanoparticles and then kept undisturbed at room temperature under ambient laboratory light conditions for 24 hours. The experiments were conducted at room temperature (~25 °C) under ambient laboratory light conditions and at the natural pH of the dye solutions without additional pH adjustment. After 24 hours, the samples were analyzed by measuring their absorbance using a UV–Visible spectrophotometer. The maximum absorption wavelength (λ_{max}) was 592 nm for crystal violet and 430 nm for bromophenol blue. The degradation efficiency was calculated using the following equation:

$$\%\ Degradation = \left(\frac{Ab_{control} - Ab_{sample}}{Ab_{control}}\right) X\ 100$$

Where, $Ab_{control}$ is the absorbance value for control while Ab_{sample} is the absorbance value of the various concentrations of nanoparticles. All degradation experiments were performed once for each catalyst dosage under identical experimental conditions.

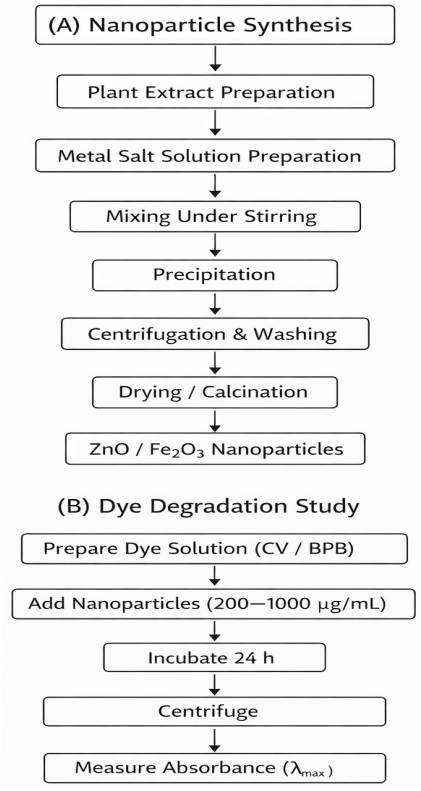

FIGURE 1. Schematic flowchart summarizing the synthesis of ZnO and Fe_2O_3 nanoparticles and the dye degradation experimental procedure

RESULT

SYNTHESIS OF THE NANOPARTICLES

Both ZnO and Fe_2O_3 nanoparticles were synthesized successfully. The appearance of black color indicates the synthesis of Fe_2O_3 (Figure 2a), whereas the brownish-yellow color indicates the formation of ZnO nanoparticles (Figure 2b).

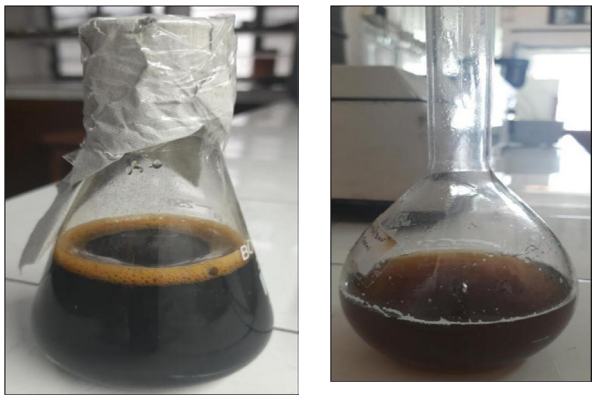

FIGURE 2. Synthesis of (a) Fe_2O_3 nanoparticles (b) ZnO nanoparticles

CHARACTERIZATION

ZINC OXIDE NANOPARTICLES

UV-VIS SPECTROSCOPY

The optical properties of nanoparticles were analyzed using UV-vis spectroscopy. The absorbance of A*egle/Zn nanoparticle* was observed within

250−800 nm wavelength. The reaction mixture showed a dark brown colour due to the stimulation of surface plasmon resonance (SPR) of ZnO nanoparticles. UV-vis absorption spectra showed a distinct absorption peak at 300 nm, confirming the synthesis of zinc oxide nanoparticles. The Tauc's plot yielded a band gap value of 3.46 eV (Figure 3).

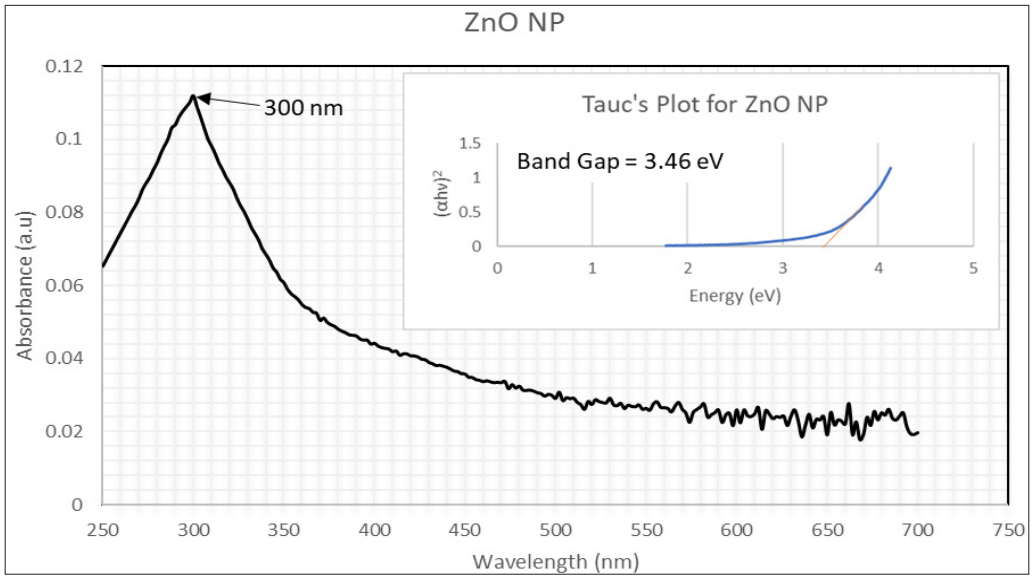

FIGURE 3. UV-vis spectrum of the synthesized ZnO nanoparticles

FTIR

The FTIR technique was used for the analysis of the chemical structures and functional groups of the ZnO nanoparticles synthesized using *Aegle* leaves extract. In Figure 4, seven prominent peaks were observed in the FTIR results at wavenumber 3450, 2348, 1743, 1630, 1460, 849 and 604 cm^{-1}. The intensity of the peak at 3450 cm^{-1} indicates an overlapping between the O-H stretching band and the N-H stretching band. At 901 cm^{-1} and 680 cm^{-1} the

peaks indicated the alkyl halide groups. The widening of these peak points towards hydrogen bonds at inter- and intra-molecular levels. At 1630 cm^{-1} the peaks can be linked to the CO vibrational stretching in residual acetates or proteins. At 1460 cm^{-1} the peak corresponds to the stretching bond of C-N in amino acids, and at 1030 cm^{-1} the peak can be linked to the bond of C-O-C that is present in the ether group of plant polysaccharides. In addition to these, the peak at 604 cm^{-1} confirms that the ZnO nanoparticles were synthesized successfully. The FTIR analysis highlights the contribution of phytochemicals in aegal leaf extract as reducing, capping, and stabilizing agents in the biosynthesized ZnO nanoparticles (Figure 4).

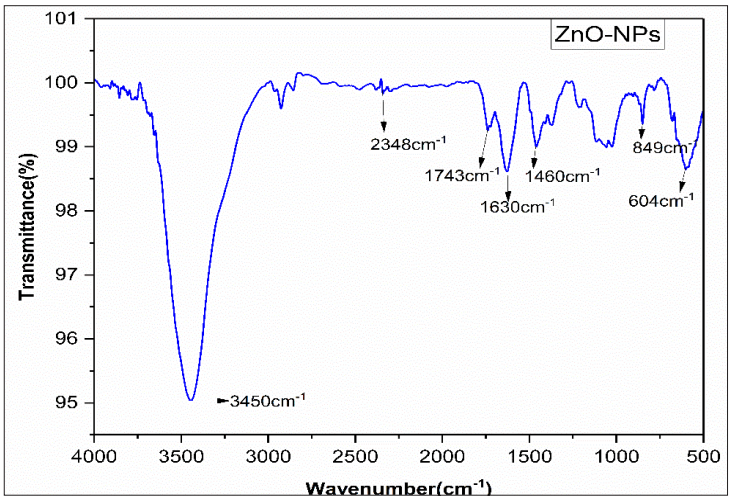

FIGURE 4. FTIR spectrum of the synthesized ZnO nanoparticles

XRD

The XRD diffractograms in Figure 5 display the nanoparticles synthesized through plant mediation. These diffractograms help us identify the ZnO nanoparticles by the (1 0 0), (0 0 2), (1 0 1), (1 0 2), (1 1 0), (1 0 3), (2 0 0), (1 1 2), and (2 0 1) crystallographic planes corresponding to the intense peaks of 2θ diffractions using JCPDS 36-1451. A well-crystalline ZnO nanoparticles is indicated by the sharp diffraction peaks. The intensity of the peaks indicates the optimum crystalline structure of ZnO Nanoparticles. The average crystallite size of the zinc oxide nanoparticles, calculated using the Scherrer equation, was 33.69 nm.

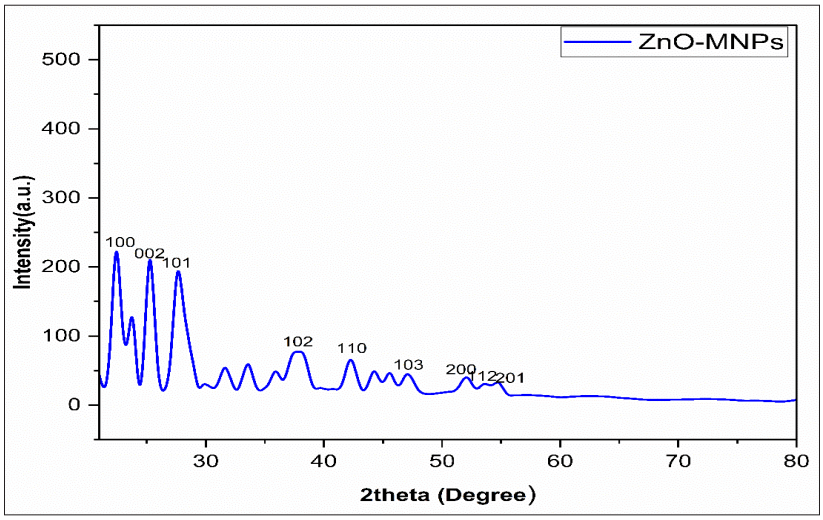

FIGURE 5. XRD spectrum of the synthesized ZnO nanoparticles

HRTEM

The morphology and structure of the ZnO nanoparticles were also investigated by TEM at varying magnifications. Figure 6, shows the TEM image which gave a clear understanding of the morphology of functionalized ZnO nanoparticles synthesized using *Aegle* leaves. The ZnO nanoparticles exhibited spherical and elongated morphologies. The average particle size measured from the TEM image was 31.952 nm which was in good agreement with the particle size calculated using the Scherrer equation.

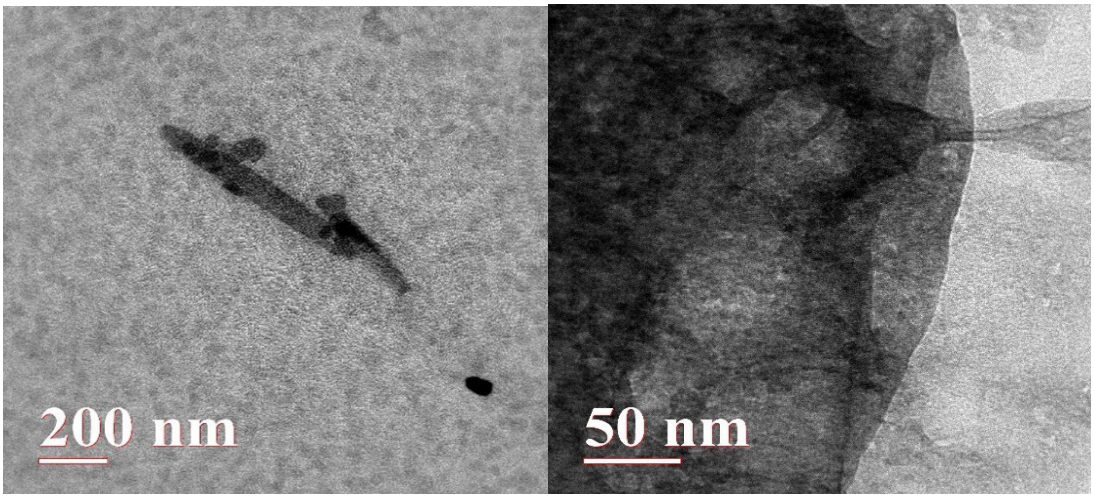

FIGURE 6. HRTEM images of the synthesized ZnO nanoparticles

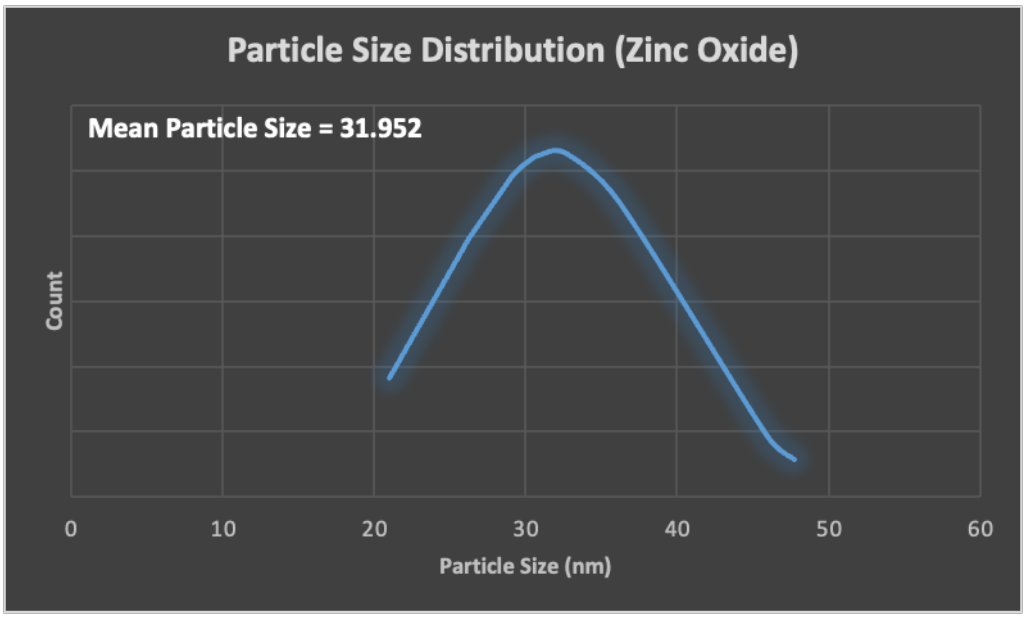

XPS

The elemental composition of the material surface and the oxidation states can be determined with the help of the XPS analysis. The spectrum peaks represent the elements present on the material surface by corresponding to the characteristic bond energies of the elements present. Shown in Figure 7 is the spectrum of XPS for the ZnO nanoparticles, pointing towards the presence of Zinc, Oxygen and Carbon. There was no contamination indicated on the surface of the sample. Due to the exposure to air, the unavoidable presence of residual carbon and C=O compounds are indicated in our sample. At the core level region of Zn-2p, the spectrum of XPS display twin peaks at about 1045 and 1022 eV corresponding to the core levels of 2p1/2 and Zn-2p3/2. The first peak can be attributed to Zn^{2+} that is present in the O deficit Zinc Oxide matrix. All the sharp peaks of Zn 2p3/2 XPS can be seen. There is an additional satellite peak also. It is therefore inferred that Zinc is present as Zn^{2+} in the ZnO lattice. The XPS of C1s showing sp^2, sp^3 & C=O.

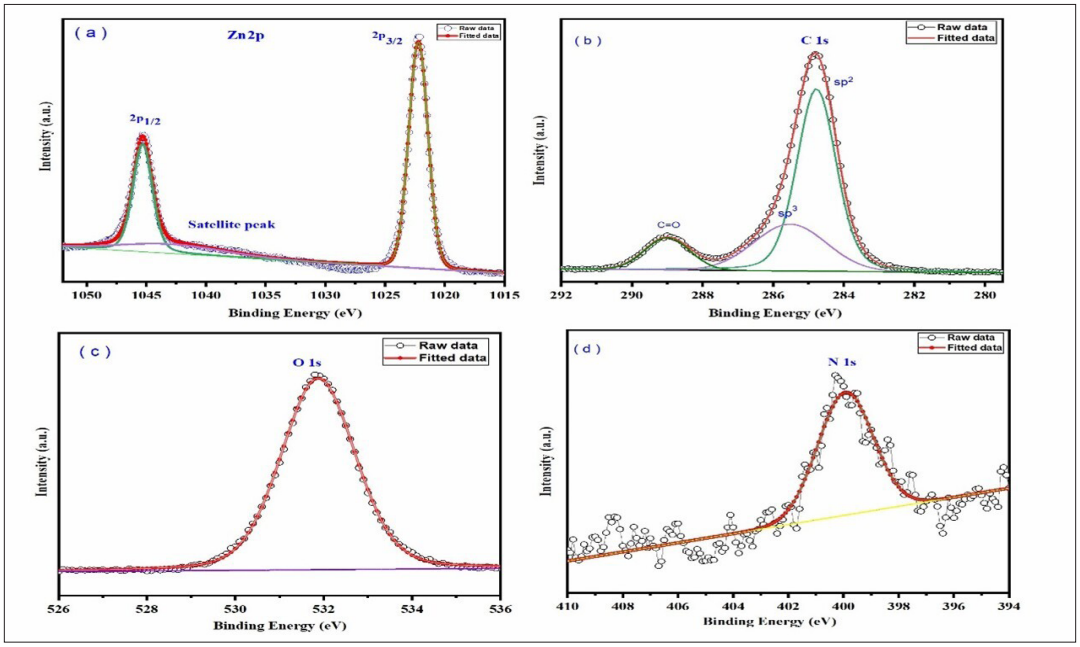

FIGURE 7. XPS spectrum of the synthesized ZnO nanoparticles

IRON OXIDE NANOPARTICLES

UV-VIS SPECTROSCOPY

The UV-Vis spectroscopy gave an absorbance peak at 228 nm. This peak in the UV region confirmed the synthesis of iron oxide nanoparticles and further indicated at the electronic transition within the nanoparticles. Using the absorbance data a Tauc's graph was plotted to determine the band gap. The band gap for iron oxide nanoparticles came out to be 3.82 eV. (Figure 8).

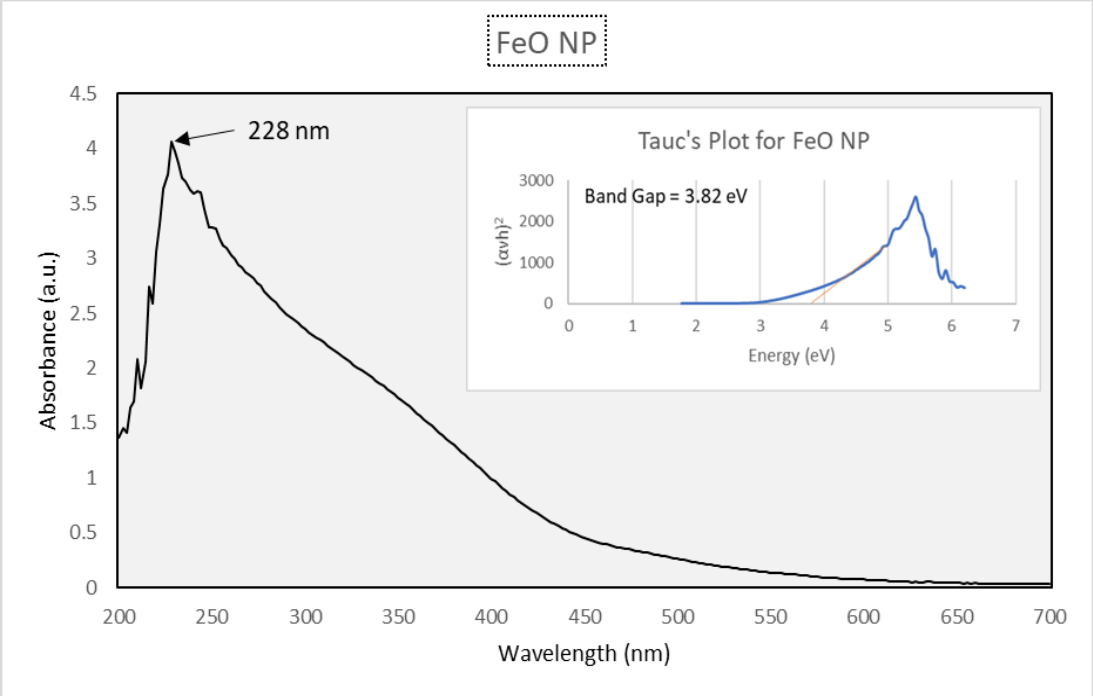

FIGURE 8. UV- vis spectrum of the synthesized Fe_2O_3

FTIR

The given spectrum depicts the peaks at various positions. The stretching and bending vibration of water molecules of certain hydroxide group on the nanoparticle's surface are identified by the peaks at 3445 cm^{-1} and 1627 cm^{-1} indicating solution-based synthesis of the nanoparticles. The 1460 cm^{-1} band indicates the CH_3 deformation. While the 597 cm^{-1} band shows the vibration of Fe_2O_3 nanoparticles (Figure 9).

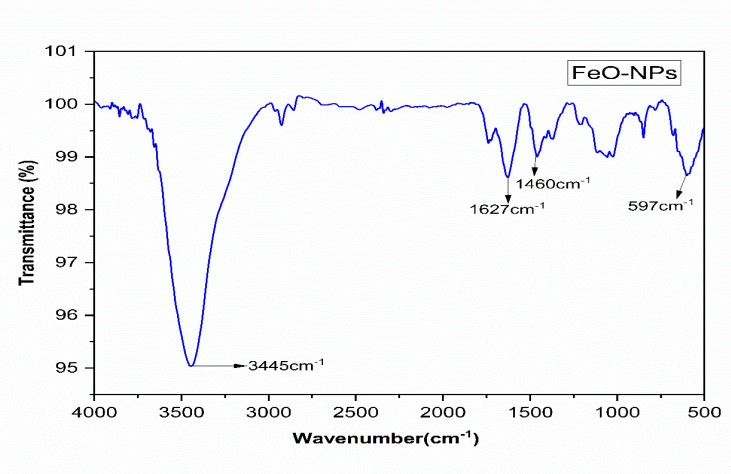

FIGURE 9: FTIR spectrum of the synthesized Fe_2O_3

XRD

Figure 10 shows the peaks of the XRD pattern for the Fe_2O_3. Using JCPDS 84-0311 the (0 1 2), (1 0 4), (1 1 0), (1 1 3), (0 2 4), (1 1 6), (2 1 4) and (3 0 0) planes were identified corresponding to the 2θ peaks indicate hematite phase of iron oxide nanoparticles. The well-crystallized hexagonal structure is confirmed by the intense peaks. The average size of the iron oxide nanoparticles calculated using the Scherrer equation came out to be 46.74 nm.

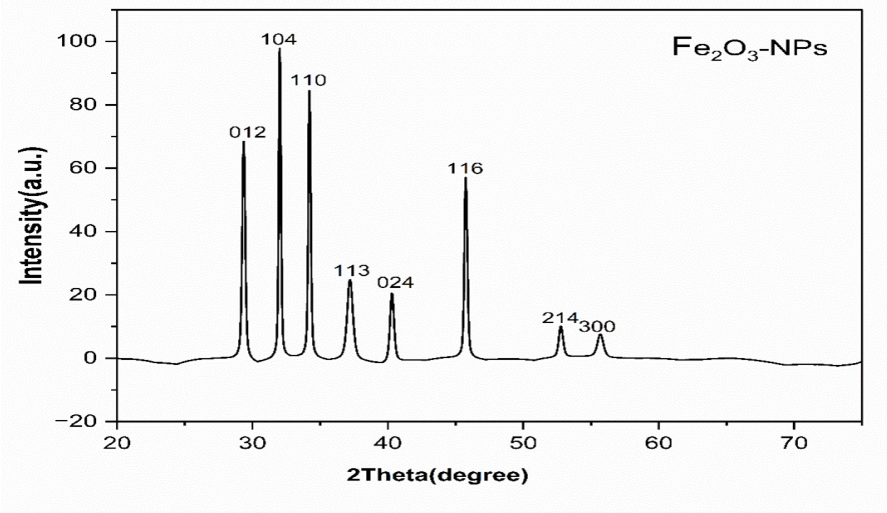

FIGURE 10. XRD spectra of the synthesized Fe_2O_3

HRTEM

HR-TEM has been carried out to get a morphological estimation, chemical composition, and crystalline structure of the synthesized Fe_2O_3 by *Mangifera indica* extract via green synthesis. The sample was cast on the copper grid and dried for two hours before the TEM analysis of the

Fe_2O_3. Spherical and rod-shaped particles are seen in the TEM images of Fe_2O_3 (Figure 11). The average size of the nanoparticles came out to be 50.286 nm which fairly agreed to the particle size calculation by Scherrer equation.

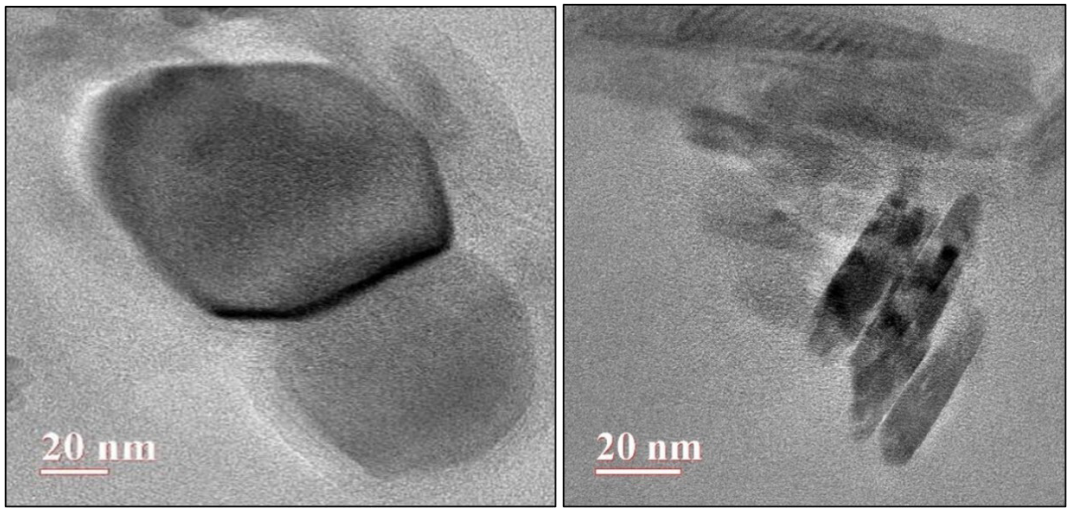

FIGURE 11. HRTEM images of the synthesized Fe_2O_3

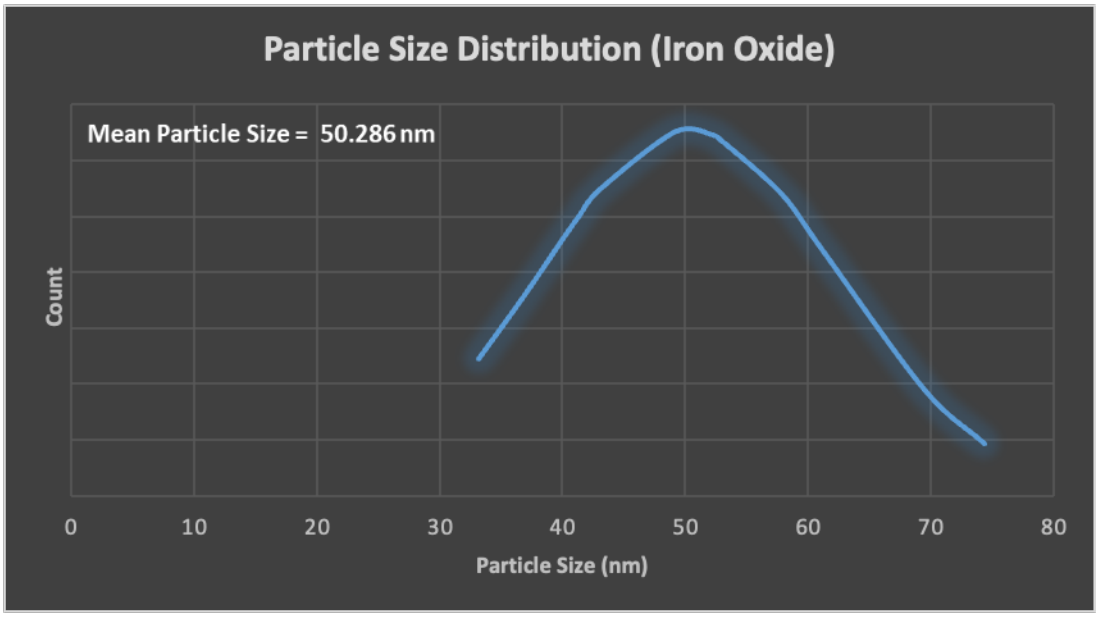

XPS

Figure 12 shows the peaks representing the O1s and Fe2p of the XPS spectra. The O1s spectrum graph represents the primary peak at 529 eV. This peak represents lattice oxygen present in Fe_2O_3. In Figure 12, the peaks of 718.6 eV and 731.8 eV respectively, correspond to the spin-orbit peaks of the $Fe2p_{3/2}$ and $Fe2p_{1/2}$ indicate the presence of Fe^{2+} and Fe^{3+} states. The XPS of C1s showing sp^2, sp^3 & C=O. The Fe 3s show binding energy at 92.97 eV. The N1s show binding energy 399.3 eV, which agrees with the presence of Fe_2O_3. Therefore, the results confirm the formation of phase-pure Fe_2O_3 nanoparticles.

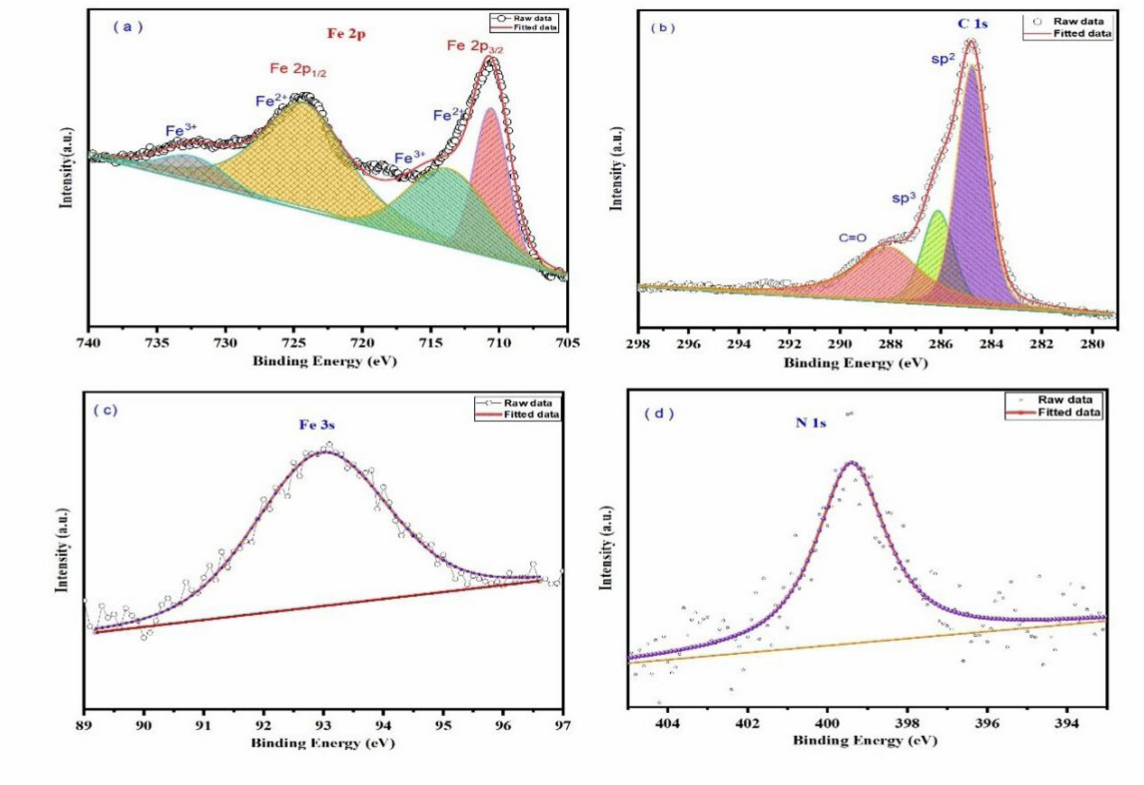

FIGURE 12. XPS spectrum of the synthesized Fe_2O_3

DYE DEGRADATION

The degradation efficiency of crystal violet (CV) and bromophenol blue (BPB) was evaluated after 24 hours of exposure to ZnO and Fe_2O_3 nanoparticles at concentrations of 200, 400, 600, 800, and 1000 µg/mL. The results indicate a dose-dependent increase in dye removal for both nanoparticles.

For crystal violet, Fe_2O_3 nanoparticles demonstrated higher degradation efficiency compared to ZnO nanoparticles. The percentage degradation of CV by Fe_2O_3 at 200, 400, 600, 800, and 1000 µg/mL was 28.25%, 41.34%, 55.47%, 68.91%, and 84.32%, respectively. In contrast, ZnO nanoparticles showed lower degradation efficiency toward CV, with corresponding removal percentages of 2.15%, 8.01%, 20.93%, 22.30%, and 24.72%.

For bromophenol blue, ZnO nanoparticles exhibited higher degradation efficiency. The percentage degradation of BPB at 200, 400, 600, 800, and 1000 µg/mL was 27.99%, 51.08%, 72.61%, 82.60%, and 98.16%, respectively. Fe_2O_3 nanoparticles did not exhibit degradation of BPB under the tested conditions. A slight increase in absorbance was observed with increasing Fe_2O_3 dosage, indicating the absence of effective removal within 24 hours.

All degradation values were calculated based on absorbance measurements obtained after 24 hours under ambient laboratory conditions.

TABLE 1. Degradation of crystal violet dye by the synthesized nanoparticles

Concentration of nanoparticles (µg/mL)	Crystal violet			
	Fe_2O_3 nanoparticles		ZnO nanoparticles	
	Absorbance	% Decrease	Absorbance	% Decrease
0	1.161		1.161	
200	0.833	28.25	1.136	2.15
400	0.681	41.34	1.068	8.01
600	0.517	55.47	0.918	20.93
800	0.361	68.91	0.902	22.30
1000	0.182	84.32	0.874	24.72

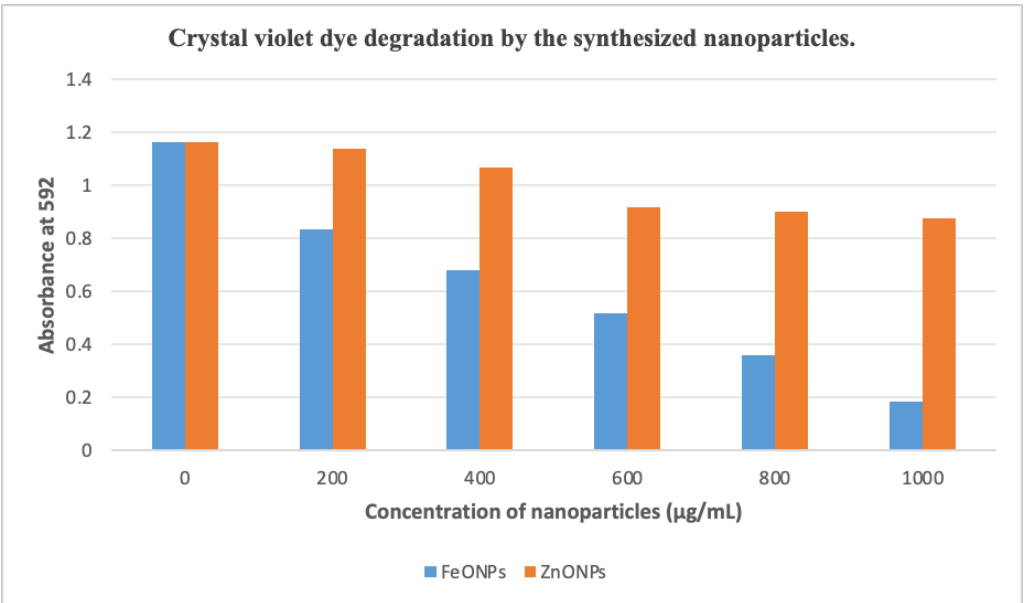

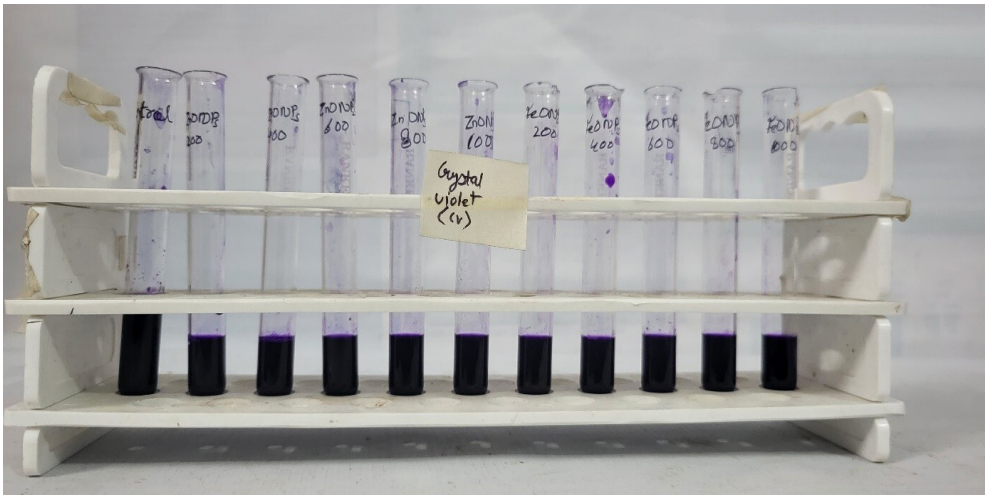

FIGURE 13. Sample with dye Before degradation (Crystal violet)

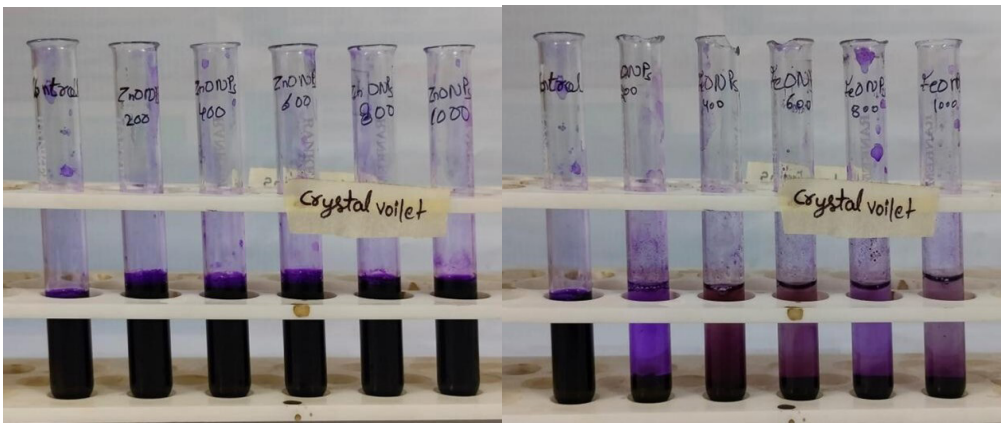

FIGURE 14. After 24 hours (Crystal violet)

TABLE 2. Degradation of Bromophenol Dye by the synthesized nanoparticles

Concentration of nanoparticles (µg/mL)	Bromophenol Blue			
	Fe_2O_3 nanoparticles		ZnO nanoparticles	
	Absorbance	% Decrease	Absorbance	% Decrease
0	1.161		1.161	
200	1.173	-1.03	0.836	27.99
400	1.181	-1.72	0.568	51.08
600	1.217	-4.82	0.318	72.61
800	1.261	-8.61	0.202	82.60
1000	1.282	-10.42	0.0214	98.16

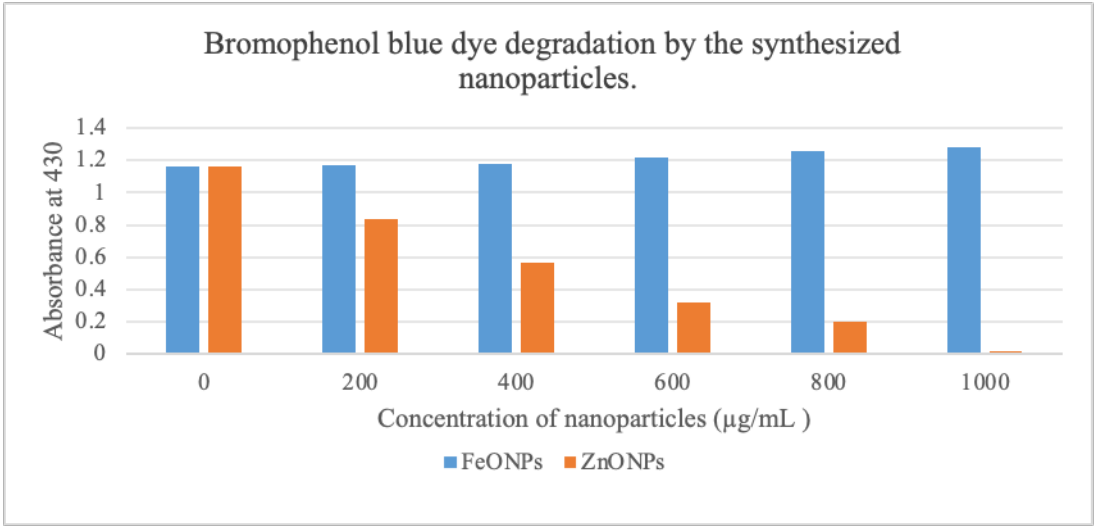

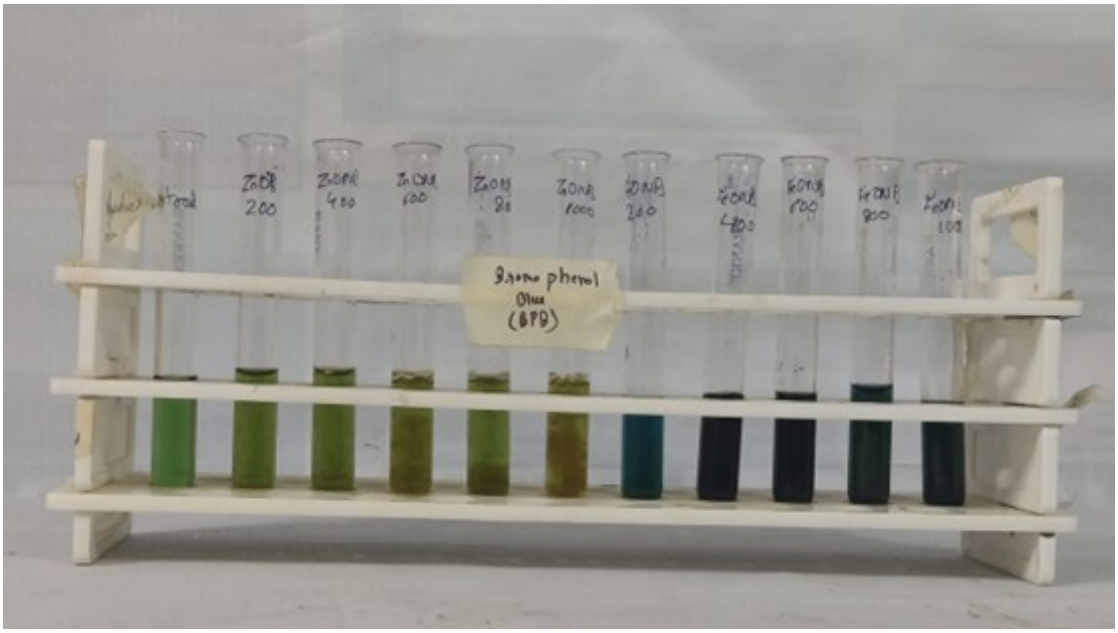

FIGURE 15. Sample with dye before degradation (Bromophenol blue)

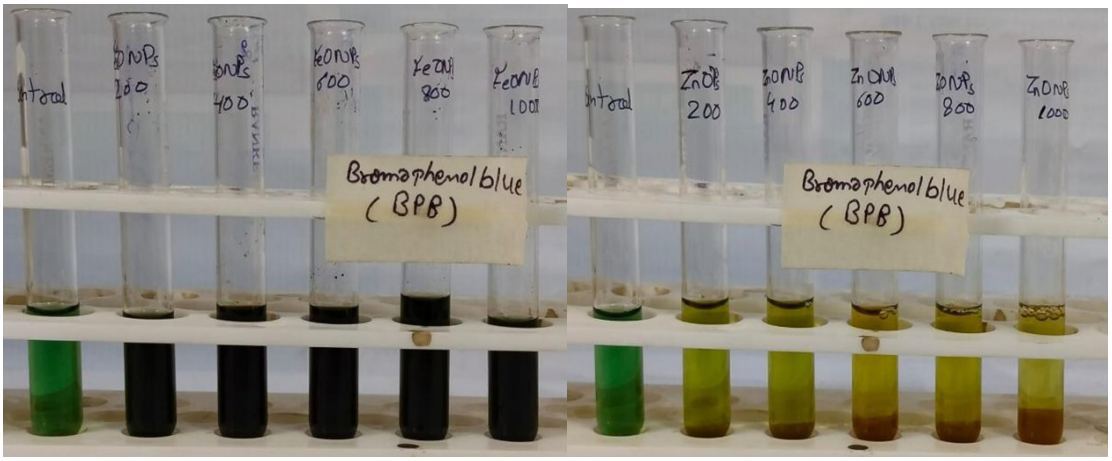

FIGURE 16. After 24 hours (Bromophenol blue)

DISCUSSION

UV–Visible spectroscopy analysis revealed characteristic absorption peaks at approximately 300 nm for ZnO nanoparticles and 228 nm for Fe_2O_3 nanoparticles, confirming their nanoscale optical behavior. The optical band gap energies were estimated using Tauc's plot analysis assuming a direct allowed electronic transition. This method follows standard optical band gap estimation using Tauc's plots in semiconductor nanomaterials (Jadhav et al. 2025). The calculated band gap values were 3.46 eV for ZnO and 3.82 eV for Fe_2O_3 nanoparticles. The higher band gap value compared to bulk Fe_2O_3 may be associated with nanoscale effects and synthesis-related variations. The comparatively lower band gap of ZnO in the present study suggests relatively easier electronic excitation under ambient light exposure, which may contribute to its enhanced degradation efficiency toward bromophenol blue. Under light irradiation, ZnO can generate electron–hole pairs that react with dissolved oxygen and water molecules to produce reactive oxygen species (ROS) such as hydroxyl and superoxide radicals, which are known to oxidize organic pollutants (Aina et al. 2025; Mahajan et al. 2025). However, as controlled light and dark experiments or radical scavenger studies were not performed, the relative contributions of photocatalytic oxidation and adsorption phenomena cannot be conclusively distinguished.

The presence of surface functional groups, as well as nanoparticle binding and coordination, was observed using the FTIR technique. FTIR results showed an important peak at 597 cm^{-1} corresponding to Fe-O stretching vibrations while peaks at 3445 cm^{-1} and 1627 cm^{-1} indicate the presence of water molecules or hydroxyl groups in the sample. Similarly, ZnO nanoparticles showed the presence of important peak at 604 cm^{-1} corresponding to Zn-O stretching vibrations while another peak at 3450 cm^{-1}, which may indicate the presence of water molecules. The presence of hydroxyl and surface functional groups may facilitate interaction between dye molecules and nanoparticle surfaces, contributing to dye removal efficiency.

XRD analysis detects the crystallographic structure of the nanoparticles and provides information about their phase composition, crystallite size, and lattice parameters. XRD analysis of Fe_2O_3 showed important peaks at 2θ values which correspond to the (0 1 2), (1 0 4), (1 1 0), (1 1 3), (0 2 4), (1 1 6), (2 1 4) and (3 0 0) planes. ZnO nanoparticles showed characteristic peaks of 2θ corresponding to the (1 0 0), (0 0 2), (1 0 1), (1 0 2), (1 1 0), (1 0 3), (2 0 0), (1 1 2), and (2 0 1) crystallographic planes of the hexagonal wurtzite structure of ZnO. The well-defined diffraction peaks confirm the crystalline nature of the synthesized nanoparticles, which is an important factor influencing their catalytic behavior.

XPS analysis provides information pertaining to elemental composition, the electronic environment of materials as well as their chemical states. XPS spectra of Fe_2O_3 showed Fe 2p3/2 and Fe 2p1/2 generally appearing at 710 and 723 eV. The oxygen atoms in the Fe_2O_3 lattice were represented by the O 1s peak, which was seen at 529 eV. Similarly, Zn 2p peaks, including Zn 2p3/2 at 1022 eV and Zn 2p1/2 around 1045 eV, were visible in the XPS spectra of ZnO nanoparticles, indicating the presence of Zn^{2+} in the ZnO lattice. The oxygen atoms in the ZnO structure were linked to the O 1s peak, which was seen at 530 eV. The presence of Fe^{3+} and Zn^{2+} oxidation states confirm the formation of Fe_2O_3 and ZnO phases, which are known to exhibit catalytic activity in dye degradation processes.

HRTEM analysis provides deeper insights into the structural and morphological characteristics of the nanoparticles. HRTEM analysis showed that Fe_2O_3

nanoparticles exhibited a spherical and rod-shaped morphology whereas ZnO nanoparticles showed a hexagonal or quasi-spherical shape. The nanoscale morphology observed through HRTEM may facilitate enhanced surface interaction between dye molecules and nanoparticle surfaces, contributing to degradation efficiency. (Alharbi et al. 2022; Ijaz et al. 2020; D. Kumar & Seth, 2021; Rana et al. 2020).

In the dye degradation studies, the performance of the nanoparticles varied depending on the dye and the type of nanoparticle. The enhanced degradation efficiency of Fe_2O_3 toward crystal violet may be associated with its crystalline structure and surface chemistry as confirmed by XRD and XPS analyses. This high degradation efficiency indicates the catalytic behavior of Fe_2O_3 nanoparticles toward crystal violet under the studied conditions. In a previous study, Fe_2O_3 were also reported to degrade methylene blue dye under basic conditions (Mahlaule-Glory et al. 2022). Similar observations of Fe_2O_3 dye degradation have been reported in recent studies, where α- Fe_2O_3 nanoparticles showed photocatalytic activity against organic dyes (Pandit et al. 2024). In the absence of added oxidants such as H_2O_2, classical Fenton-like reactions are unlikely to dominate under the studied conditions (Saif et al. 2016). Therefore, the observed degradation of crystal violet by Fe_2O_3 may involve surface-mediated redox interactions and adsorption-assisted catalytic processes rather than a conventional Fenton pathway. However, Fe_2O_3 nanoparticles did not exhibit effective degradation of bromophenol blue under the experimental conditions. A slight increase in absorbance was observed with increasing Fe_2O_3 concentration. This behaviour may be attributed to light scattering effects at higher nanoparticle dosages, nanoparticle–dye interactions altering the optical properties of the solution, or possible surface complex formation influencing spectrophotometric measurements rather than actual chemical degradation (Mahmoodi et al. 2011).

On the other hand, the enhanced performance of ZnO toward bromophenol blue may be attributed to its photocatalytic properties under ambient light conditions, although the relative contributions of adsorption and photocatalytic processes were not independently evaluated in this study. The lower band gap value (3.46 eV) supports its potential for light-induced catalytic activity, which may facilitate oxidative degradation of the dye molecules. These findings are consistent with previous reports demonstrating effective photocatalytic degradation of organic dyes using ZnO nanoparticles under light exposure (Mahajan et al. 2025). In a similar study, green synthesized ZnO nanoparticles achieved 98.50 % degradation efficiency toward bromophenol blue (Venkatesan et al. 2024).

While green synthesis of ZnO and Fe_2O_3 nanoparticles has been previously reported, the present study provides a comparative evaluation of their dye-specific degradation performance under identical experimental conditions, highlighting their selective applicability. The differences in performance between ZnO nanoparticles and Fe_2O_3 highlight the importance of selecting appropriate nanoparticles based on the target pollutant and the desired treatment conditions. The results suggest that a combination of ZnO and Fe_2O_3 nanoparticles could potentially be used in a complementary manner to address a wider range of organic pollutants in wastewater treatment applications.

The present study evaluated dye degradation efficiency based on end-point absorbance measurements after 24 hours. Kinetic modeling and intermediate time-point analyses were not performed and may be considered in future investigations to provide deeper insight into degradation mechanisms.

Overall, the findings demonstrate the potential applicability of biologically synthesized nanoparticles for dye removal under laboratory conditions.

CONCLUSION

The study demonstrated that Fe_2O_3 nanoparticles showed optimal performance in crystal violet degradation (up to 84.32%), whereas ZnO nanoparticles were highly efficient for bromophenol blue degradation (up to 98.15%), suggesting their complementary application in wastewater remediation.

ACKNOWLEDGEMENT

Author would like to thank University of Rajasthan, Jaipur for supporting this work.

DECLARATION OF COMPETING INTEREST

None.

REFERENCES

Aina, A. R. N., Patel, H., Aich, S., Roy, B., Samanta, N. S. & Pal, B. 2025. Recent advances in ZnO based photocatalysts for industrial dye degradation. *Discover Applied Sciences* 7(9): 977. https://doi.org/10.1007/s42452-025-07530-z

Akintelu, S. A. & Folorunso, A. S. 2020. A review on green synthesis of zinc oxide nanoparticles using plant extracts and its biomedical applications. *BioNanoScience* 10(4): 848-863. https://doi.org/10.1007/s12668-020-00774-6

Alharbi, N. S., Alsubhi, N. S. & Felimban, A. I. 2022. Green synthesis of silver nanoparticles using medicinal plants: Characterization and application. *Journal of Radiation Research and Applied Sciences* 15(3): 109-124. https://doi.org/10.1016/j.jrras.2022.06.012

Bibi, I., Nazar, N., Iqbal, M., Kamal, S., Nawaz, H., Nouren, S., Safa, Y., Jilani, K., Sultan, M., Ata, S., Rehman, F. & Abbas, M. 2017. Green and eco-friendly synthesis of cobalt-oxide nanoparticle: Characterization and photo-catalytic activity. *Advanced Powder Technology* 28(9): 2035-2043. https://doi.org/10.1016/j.apt.2017.05.008

Biesinger, M. C. 2017. Advanced analysis of copper X-ray photoelectron spectra. *Surface and Interface Analysis* 49(13): 1325-1334. https://doi.org/10.1002/sia.6239

Ebrahiminezhad, A., Zare-Hoseinabadi, A., Sarmah, A. K., Taghizadeh, S., Ghasemi, Y. & Berenjian, A. 2018. Plant-mediated synthesis and applications of iron nanoparticles. *Molecular Biotechnology* 60(2): 154-168. https://doi.org/10.1007/s12033-017-0053-4

Gordon, B., Boisson, S., Johnston, R., Trouba, D. J. & Cumming, O. 2023. Unsafe water, sanitation and hygiene: A persistent health burden. *Bulletin of the World Health Organization* 101(9): 551. https://doi.org/10.2471/BLT.23.290668

Ijaz, I., Gilani, E., Nazir, A. & Bukhari, A. 2020. Detail review on chemical, physical and green synthesis, classification, characterizations and applications of nanoparticles. *Green Chemistry Letters and Reviews* 13(3): 59-81. https://doi.org/10.1080/17518253.2020.1802517

Iravani, S. 2011. Green synthesis of metal nanoparticles using plants. *Green Chemistry* 13(10): 2638-2650. https://doi.org/10.1039/c1gc15386b

Jadhav, V., Dhanwate, Y., Raut, P., Shinde, S., Sawant, R. & Bhagare, A. 2025. Efficient photocatalytic methylene blue dye degradation from green-synthesized silver-doped iron oxide ($Ag@Fe_2O_3$) nanostructures. *Discover Nano* 20(1): 66. https://doi.org/10.1186/s11671-025-04242-6

Kant, R. 2012. Textile dyeing industry an environmental hazard. *Natural Science* 4(1): 22-26. https://doi.org/10.4236/ns.2012.41004

Kaur, P., Thakur, R., Malwal, H., Manuja, A. & Chaudhury, A. 2018. Biosynthesis of biocompatible and recyclable silver/iron and gold/iron core-shell nanoparticles for water purification technology. *Biocatalysis and Agricultural Biotechnology* 14: 189-197. https://doi.org/10.1016/j.bcab.2018.03.002

Kolodziejczak-Radzimska, A. & Jesionowski, T. 2014. Zinc oxide - from synthesis to application: A review. *Materials* 7(4): 2833-2881. https://doi.org/10.3390/ma7042833

Kovacs, I., Vereb, G., Kertesz, S., Hodur, C. & Laszlo, Z. 2018. Fouling mitigation and cleanability of TiO2 photocatalyst-modified PVDF membranes during ultrafiltration of model oily wastewater with different salt contents. *Environmental Science and Pollution Research International* 25(35): 34912-34921. https://doi.org/10.1007/s11356-017-0998-7

Kumar, D. & Seth, C. S. 2021. Green-synthesis, characterization, and applications of nanoparticles (NPs): A mini review. *International Journal of Plant and Environment* 7(1): 91-95. https://doi.org/10.18811/ijpen.v7i01.11

Kumar, G. V., Dinesh Gokavarapu, S., Rajeswari, A., Stalin Dhas, T., Karthick, V., Kapadia, Z., Shrestha, T., Barathy, I. A., Roy, A. & Sinha, S. 2011. Facile green synthesis of gold nanoparticles using leaf extract of antidiabetic potent Cassia auriculata. *Colloids and Surfaces B: Biointerfaces* 87(1): 159-163. https://doi.org/10.1016/j.colsurfb.2011.05.016

Mahajan, M., Kumar, S., Gaur, J., Kaushal, S., Dalal, J., Singh, G., Misra, M. & Ahlawat, D. S. 2025. Green synthesis of ZnO nanoparticles using Justicia adhatoda for photocatalytic degradation of malachite green and reduction of 4-nitrophenol. *RSC Advances* 15(4): 2958-2980. https://doi.org/10.1039/d4ra08632e

Mahdavi, M., Ahmad, M. B., Haron, M. J., Namvar, F., Nadi, B., Ab Rahman, M. Z. & Amin, J. 2013. Synthesis, surface modification and characterisation of biocompatible magnetic iron oxide nanoparticles for biomedical applications. *Molecules* 18(7): 7533-7548. https://doi.org/10.3390/molecules18077533

Mahlaule-Glory, L. M., Mapetla, S., Makofane, A., Mathipa, M. M. & Hintsho-Mbita, N. C. 2022. Biosynthesis of iron oxide nanoparticles for the degradation of methylene blue dye, sulfisoxazole antibiotic and removal of bacteria from real water. *Heliyon* 8(9): e10536. https://doi.org/10.1016/j.heliyon.2022.e10536

Mahmoodi, N. M., Salehi, R., Arami, M. & Bahrami, H. 2011. Dye removal from colored textile wastewater using chitosan in binary systems. *Desalination* 267(1): 64-72. https://doi.org/10.1016/j.desal.2010.09.007

Nagar, N. & Devra, V. 2019. A kinetic study on the degradation and biodegradability of silver nanoparticles catalyzed Methyl Orange and textile effluents. *Heliyon* 5(3): e01356. https://doi.org/10.1016/j.heliyon.2019.e01356

Pandit, U., Rama, V., Jadhav, P., Ganesh, K., Sakharam Jawale, Vivekanand Mangal, Dubepatil, R., Gurao, R. & Late, D. J. 2024. Synthesis and characterization of micro-/nano-alpha-Fe_2O_3 for photocatalytic dye

degradation. *RSC Advances* 14(40): 29099-29105. https://doi.org/10.1039/d4ra04575k

Patterson, A. L. 1939. The Scherrer formula for X-ray particle size determination. *Physical Review* 56(10): 978. https://doi.org/10.1103/PhysRev.56.978

Ramesh, M., Anbuvannan, M. & Viruthagiri, G. 2015. Green synthesis of ZnO nanoparticles using Solanum nigrum leaf extract and their antibacterial activity. *Spectrochimica Acta Part A: Molecular and Biomolecular Spectroscopy* 136(PB): 864-870. https://doi.org/10.1016/j.saa.2014.09.105

Rana, A., Yadav, K. & Jagadevan, S. 2020. A comprehensive review on green synthesis of nature-inspired metal nanoparticles: Mechanism, application and toxicity. *Journal of Cleaner Production* 272: 122880. https://doi.org/10.1016/j.jclepro.2020.122880

Razavi, R., Amiri, M., Alshamsi, H. A., Eslaminejad, T. & Salavati-Niasari, M. 2021. Green synthesis of Ag nanoparticles in oil-in-water nano-emulsion and evaluation of their antibacterial and cytotoxic properties as well as molecular docking. *Arabian Journal of Chemistry* 14(9): 103323. https://doi.org/10.1016/j.arabjc.2021.103323

Ritu, Verma, K. K., Das, A. & Chandra, P. 2023. Phytochemical-based synthesis of silver nanoparticle: Mechanism and potential applications. *BioNanoScience* 13(3): 1359-1380. https://doi.org/10.1007/s12668-023-01125-x

Saif, S., Tahir, A. & Chen, Y. 2016. Green synthesis of iron nanoparticles and their environmental applications and implications. *Nanomaterials* 6(11): 209. https://doi.org/10.3390/nano6110209

Singh, J., Chang, Y. Y., Koduru, J. R., Yang, J. K. & Singh, D. P. 2017. Rapid Fenton-like degradation of methyl orange by ultrasonically dispersed nano-metallic particles. *Environmental Engineering Research* 22(3): 245-254. https://doi.org/10.4491/eer.2016.138

Singh, J. & Dhaliwal, A. S. 2020. Plasmon-induced photocatalytic degradation of methylene blue dye using biosynthesized silver nanoparticles as photocatalyst. *Environmental Technology* 41(12): 1520-1534. https://doi.org/10.1080/09593330.2018.1540663

Soni, S., Kumari, A., Sharma, S., Sharma, A., Sheel, V., Thakur, R., Bhatia, S. K. & Sharma, A. K. 2025. Recent advances in metal (M = Ni/Fe/Cu/Zn) oxide nanomaterials-mediated removal of dyes from wastewater. *Journal of the Taiwan Institute of Chemical Engineers* 166: 105565. https://doi.org/10.1016/j.jtice.2024.105565

Tripathi, M., Singh, S., Pathak, S., Kasaudhan, J., Mishra, A., Bala, S., Garg, D., Singh, R., Singh, P., Singh, P. K., Shukla, A. K. & Pathak, N. 2023. Recent strategies for the remediation of textile dyes from wastewater: A systematic review. *Toxics* 11(11): 940. https://doi.org/10.3390/toxics11110940

Venkatesan, S., Suresh, S., Arumugam, J., Ramu, P., Pugazhenthiran, N., Jothilakshmi, R. & Prabu, K. M. 2024. Sunlight assisted degradation of methylene blue dye by zinc oxide nanoparticles green synthesized using Vitex negundo plant leaf extract. *Results in Chemistry* 7: 101315. https://doi.org/10.1016/j.rechem.2024.101315

Vereb, G., Kassai, P., Nascimben Santos, E., Arthanareeswaran, G., Hodur, C. & Laszlo, Z. 2020. Intensification of the ultrafiltration of real oil-contaminated (produced) water with pre-ozonation and/or with TiO2, TiO2/CNT nanomaterial-coated membrane surfaces. *Environmental Science and Pollution Research International* 27(18): 22195-22205. https://doi.org/10.1007/s11356-020-08047-1

Yadwade, R., Kirtiwar, S. & Ankamwar, B. 2021. A review on green synthesis and applications of iron oxide nanoparticles. *Journal of Nanoscience and Nanotechnology* 21(12): 5812-5834. https://doi.org/10.1166/jnn.2021.19285